PALEOCEANOGRAPHY, VOL. 28, 237–252, doi:10.1002/palo.20024, 2013

Calibration and application of B/Ca, Cd/Ca, and $\delta^{11}B$ in *Neogloboquadrina pachyderma* (sinistral) to constrain CO_2 uptake in the subpolar North Atlantic during the last deglaciation

Jimin Yu,[1,2] David J. R. Thornalley,[3] James W. B. Rae,[4,5] and Nick I. McCave[6]

Received 26 November 2012; revised 18 February 2013; accepted 22 February 2013; published 30 May 2013.

[1] The North Atlantic and Norwegian Sea are prominent sinks of atmospheric CO_2 today, but their roles in the past remain poorly constrained. In this study, we attempt to use B/Ca and $\delta^{11}B$ ratios in the planktonic foraminifera *Neogloboquadrina pachyderma* (sinistral variety) to reconstruct subsurface water pH and pCO_2 changes in the polar North Atlantic during the last deglaciation. Comparison of core-top results with nearby hydrographic data shows that B/Ca in *N. pachyderma* (s) is mainly controlled by seawater $B(OH)_4^-/HCO_3^-$ with a roughly constant partition coefficient $\left(K_D = \frac{[B/Ca]_{CaCO_3}}{[B(OH)_4^-/HCO_3^-]_{seawater}}\right)$ of $1.48 \pm 0.15 \times 10^{-3}$ (2σ), and $\delta^{11}B$ in this species is offset below $\delta^{11}B$ of the borate in seawater by 3.38 ± 0.71‰ (2σ). These values represent our best estimates with the sparse available hydrographic data close to our core-tops. More culturing and sediment trap work is needed to improve our understanding of boron incorporation into *N. pachyderma* (s). Application of a constant K_D of 1.48×10^{-3} to high resolution *N. pachyderma* (s) B/Ca records from two adjacent cores off Iceland shows that subsurface pCO_2 at the habitat depth of *N. pachyderma* (s) (~50 m) generally followed the atmospheric CO_2 trend but with negative offsets of ~10–50 ppmv during 19–10 ka. These B/Ca-based reconstructions are supported by independent estimates from low-resolution $\delta^{11}B$ measurements in the same cores. We also calibrate and apply Cd/Ca in *N. pachyderma* (s) to reconstruct nutrient levels for the same down cores. Like today's North Atlantic, past subsurface pCO_2 variability off Iceland was significantly correlated with nutrient changes that might be linked to surface nutrient utilization and mixing within the upper water column. Because surface pCO_2 (at 0 m water depth) is always lower than at deeper depths and if the application of a constant K_D is valid, our results suggest that the polar North Atlantic has remained a CO_2 sink during the calcification seasons of *N. pachyderma* (s) over the last deglaciation.

Citation: Yu, J., D. J. R. Thornalley, J. W. B. Rae, and N. I. McCave (2013), Calibration and application of B/Ca, Cd/Ca, and $\delta^{11}B$ in *Neogloboquadrina pachyderma* (sinistral) to constrain CO_2 uptake in the subpolar North Atlantic during the last deglaciation, *Paleoceanography*, *28*, 237–252, doi:10.1002/palo.20024.

1. Introduction

[2] Natural variations in atmospheric CO_2 are primarily governed by gas exchange with the land biosphere and ocean, whose carbon reservoirs are respectively ~3 and ~50 times that of the atmosphere [*Sigman and Boyle*, 2000]. Mapping of surface seawater partial pressure of CO_2 (pCO_2) in the modern ocean [*Takahashi et al.*, 2009] shows that low-latitude regions, such as the eastern equatorial Pacific and Arabian Sea, serve as CO_2 sources to the atmosphere due to upwelling and warming of nutrient- and CO_2-rich subsurface mode waters primarily sourced from Southern Ocean [*Sarmiento et al.*, 2003]. As the upwelled waters flow to high latitudes, cooling and nutrient utilization draw down surface water pCO_2, producing prominent CO_2 sinks at subtropical/subpolar confluence regions that absorb CO_2 from the atmosphere in both hemispheres [*Takahashi et al.*, 2009]. On centennial to millennial timescales, which are sufficiently long to complete the shallow mode water

All supporting information may be found in the online version of this article.

[1]Research School of Earth Sciences, The Australian National University, Canberra, ACT, Australia.
[2]Lawrence Livermore National Laboratory, Livermore, California, USA.
[3]Woods Hole Oceanographic Institution, Woods Hole, Massachusetts, USA.
[4]Division of Geological and Planetary Sciences, California Institute of Technology, Pasadena, California, USA.
[5]Bristol Isotope Group, Department of Earth Sciences, University of Bristol, Bristol, UK.
[6]The Godwin Laboratory for Palaeoclimate Research, Department of Earth Sciences, University of Cambridge, Cambridge, UK.

Corresponding author: J. Yu, Research School of Earth Sciences, The Australian National University, Canberra, ACT 0200, Australia. (jimin.yu@anu.edu.au)

0883-8305/13/10.1002/palo.20024

circulation, CO_2 degassing at low-latitude upwelling regions roughly balances CO_2 absorption at subtropical/subpolar convergence zones, resulting in little net effect on atmospheric CO_2 content [*Hain et al*., 2013; *Sarmiento et al*., 2003]. Therefore, the most likely regions that could have significant impacts on atmospheric CO_2 on millennial or longer timescales are the polar oceans [*Sigman and Boyle*, 2000]. These regions are crucial for carbon exchange between the deep ocean and the surface ocean and the atmosphere, due to their tight link to the deep ocean circulation, which occurs on the timescale of ~1000 years [*Broecker*, 1982].

[3] The cause of the rapid rise of 75 parts per million in volume (ppmv) in atmospheric CO_2 during the last deglaciation has been suggested to be CO_2 release by intensified upwelling in the Southern Ocean [e.g., *Anderson et al*., 2009]. Release of CO_2 from the Southern Ocean to the atmosphere also occurred during the most recent pre-industrial period [*Keeling and Heimann*, 1986]. However, no rise in atmospheric CO_2 was observed [*Etheridge et al*., 1996], as CO_2 released from the Southern Ocean was largely balanced by CO_2 uptake in the North Atlantic [*Broecker and Peng*, 1992]. This highlights the point that, in addition to constraining variation in potential CO_2 source regions (e.g., Southern Ocean), quantification of CO_2 flux in oceanic sinks (e.g., North Atlantic) is critical to understanding past atmospheric CO_2 changes.

[4] Direct constraints on past changes in CO_2 source-fluxes and sink-fluxes in the polar oceans are lacking, primarily due to the shortage of surface water pCO_2 reconstructions in cold high-latitude waters. Surface water pCO_2 in the North Atlantic has been reconstructed using organic matter within planktonic foraminifera, but this method is complicated by having to use planktonic $\delta^{13}C$ to obtain a surface water value and gives unreasonably high sea-air pCO_2 gradients (ΔpCO_2) of up to approximately −100 ppmv based on core-top samples from the North Atlantic [*Jasper et al*., 1995; *Maslin et al*., 1997]. It is also unclear which seasons are represented by these pCO_2 reconstructions. Although yielding more reasonable results, the recent estimation method based on planktonic foraminifera weight [*Barker and Elderfield*, 2002] has been challenged [e.g., *Beer et al*., 2010]. As a result, we do not know whether the polar North Atlantic has served as a sink or a source of CO_2 to the atmosphere in the past. In this study, we explore the feasibility of using B/Ca and $\delta^{11}B$ in the planktonic foraminifera *Neogloboquadrina pachyderma* (sinistral) as novel proxies for cold polar subsurface water pCO_2 reconstructions. We present the first high-resolution B/Ca-based estimates of subsurface water pCO_2 during the last deglaciation (19–10 ka) in the subpolar/polar North Atlantic, using two cores south of Iceland. We have also examined Cd/Ca in *N. pachyderma* (s) to investigate possible links between subsurface water nutrient changes and pCO_2 in the past.

2. B/Ca and $\delta^{11}B$ Methodology

[5] The use of foraminiferal B/Ca and $\delta^{11}B$ for seawater pH and pCO_2 reconstructions has been discussed previously [*Foster*, 2008; *Hemming and Hanson*, 1992; *Hönisch and Hemming*, 2005; *Palmer et al*., 2010; *Rae et al*., 2011; *Sanyal et al*., 1996; *Yu et al*., 2007b]. Briefly, dissolved boron in seawater exists primarily as a mixture of the mononuclear species $B(OH)_3$ (boric acid) and $B(OH)_4^-$ (borate), the proportions of which are highly pH dependent. Boron has two stable isotopes, ^{11}B and ^{10}B, and an equilibrium isotope fractionation occurs between $B(OH)_3$ and $B(OH)_4^-$ [*Klochko et al*., 2006]. The $^{11}B/^{10}B$ ratio, expressed in delta notation as $\delta^{11}B$, of each molecular species is thus also pH dependent. $\delta^{11}B$ data from modern marine carbonates suggest that $B(OH)_4^-$ is the dominant species incorporated into carbonates [*Hemming and Hanson*, 1992]:

$$CaCO_3 + B(OH)_4^- \rightarrow Ca(HBO_3) + HCO_3^- + H_2O \quad (1)$$

[6] Both the boron concentration and isotopic ratio in carbonates will thus be a function of the ocean carbonate system. $\delta^{11}B$ in carbonates ($\delta^{11}B_{cc}$) can be used to calculate seawater pH by

$$pH = pK_B^* - \log\left(-\frac{\delta^{11}B_{sw} - \left(\delta^{11}B_{cc} - \delta^{11}B_{cc-B4}\right)}{\delta^{11}B_{sw} - \alpha.\ \delta^{11}B_{cc} - 1000\cdot(\alpha-1)}\right) \quad (2)$$

where pK_B^* is the pK value for boric acid at the in situ temperature and salinity, $\delta^{11}B_{sw} = 39.61‰$ [*Foster et al*., 2010], $\alpha = 27.2‰$ [*Klochko et al*., 2006], and $\delta^{11}B_{cc\text{-}B4}$ is the offset between $\delta^{11}B_{cc}$ and $\delta^{11}B$ of seawater $B(OH)_4^-$. The partition coefficient, K_D, of boron between calcium carbonate and seawater is defined as

$$K_D = \frac{[B/Ca]_{CaCO_3}}{\left[B(OH)_4^-/HCO_3^-\right]_{seawater}} \quad (3)$$

[7] Provided that the K_D in equation (2) is constant or can be quantified, carbonate B/Ca ratios can be used to estimate seawater $[B(OH)_4^-/HCO_3^-]$. Coupled with an estimate of surface water alkalinity (ALK), B/Ca-derived $[B(OH)_4^-/HCO_3^-]$ ratios and $\delta^{11}B$-derived pH provide constraints on seawater pCO_2. Given the close relationships in the carbonate system between pH, $[B(OH)_4^-/HCO_3^-]$, and $[CO_2]$, these pCO_2 estimates are relatively insensitive to the alkalinity estimate and will be mainly driven by the B/Ca and $\delta^{11}B$ data [*Foster*, 2008; *Hönisch et al*., 2008; *Palmer and Pearson*, 2003].

[8] Previous measurements of B/Ca in *Globigerina bulloides*, *Globigerina inflata*, *Globigerinoides ruber*, and *Globigerinoides sacculifer* suggest that K_D varies within and between these planktonic species as a result of secondary controls by temperature or carbonate ion concentration [*Foster*, 2008; *Yu et al*., 2007b]. Approaches have been suggested to estimate seawater $[B(OH)_4^-/HCO_3^-]$ and hence pH and pCO_2, although corrections for temperature or carbonate ion effect inevitably introduce errors in the calculated pCO_2 values and compromise interpretations [*Yu et al*., 2007b]. Recent work [*Allen and Hönisch*, 2012] has also suggested that the variability of K_D associated with some species such as *G. bulloides*, *G. ruber*, and *G. sacculifer* could mainly be driven by the denominator in equation (3), not by B/Ca itself, casting doubt on previous paleoreconstructions [e.g., *Palmer et al*., 2010; *Yu et al*., 2007b]. *Allen and Hönisch* [2012] also stressed the potential risk of using down-core samples to calibrate K_D.

[9] In this study, we first explore the variability of K_D in the planktonic foraminifera *N. pachyderma* (s) using core-tops from the North Atlantic. We then apply the core-top derived K_D to two down-core records and check the credibility of our

estimates of K_D for paleo-pH and pCO_2 reconstructions by comparing reconstructions from a second pH proxy, $\delta^{11}B$, from the same cores.

3. Species, Materials, and Methods

[10] During cold time intervals, the dominant species in polar and subpolar waters is *N. pachyderma* (s). Other planktonic foraminifera species are therefore either absent or very low in abundance (≲2% of the total foraminiferal assemblage) in subpolar and polar North Atlantic cores throughout the LGM and cold intervals of the deglacial. *N. pachyderma* (s) is thus widely used for paleoceanographic studies to obtain continuous glacial-interglacial records in this region. Here, we explore the possibility of using B/Ca and $\delta^{11}B$ ratios in *N. pachyderma* (s) for past subsurface water pH and pCO_2 reconstructions. Core-top samples include three locations from the southern Norwegian Sea, two locations from the South Iceland Basin, and 12 locations from the Labrador Sea (Figure 1 and Table 1). These core-tops are verified to be of recent age (≲3000 years), mostly based on ^{14}C dates [*Kristjánsdóttir et al.*, 2011]. Two nearby cores RAPiD-10-1P (62°58.53'N, 17°35.37W; 1237 m water depth) and RAPiD-15-4P (62°17.58'N, 17°08.04W; 2133 m water depth) (hereafter 1P and 4P, respectively) from the South Iceland Rise were used for down-core B/Ca and $\delta^{11}B$

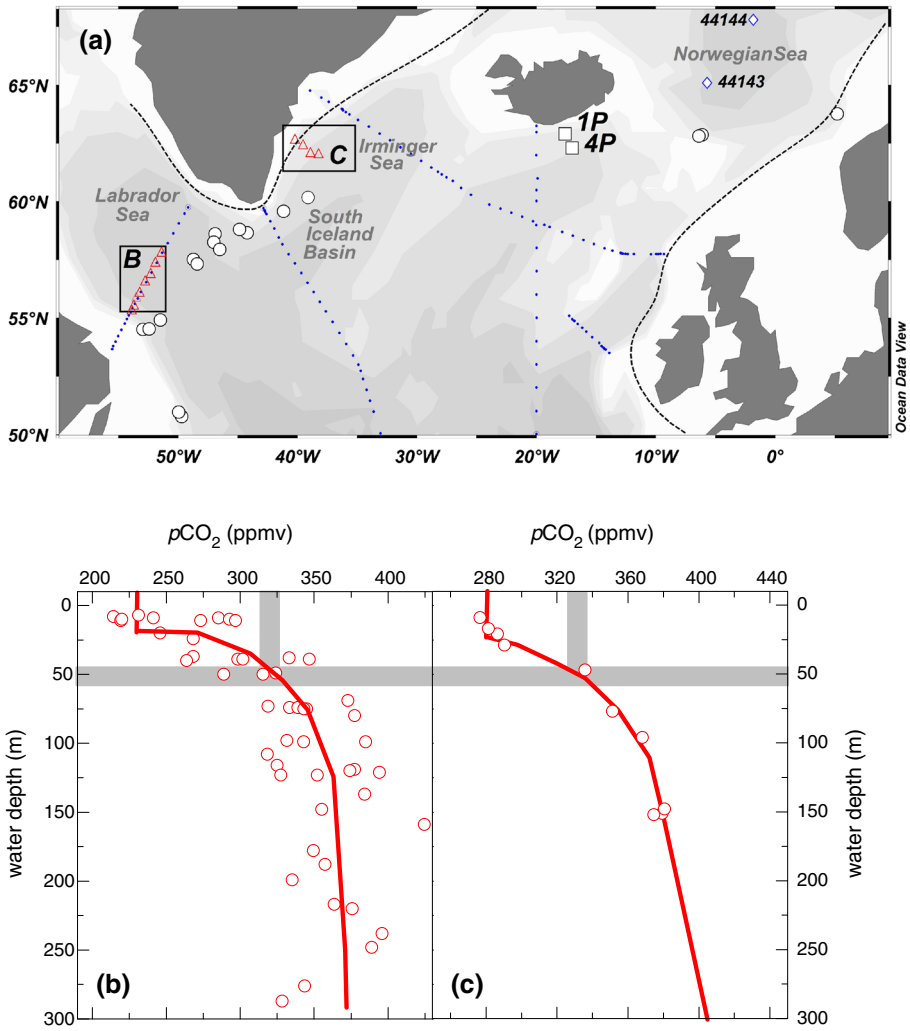

Figure 1. (a) Map showing locations of core-tops (circles), down cores (squares), hydrographic sites (dots, diamonds, and triangles) used in this study. Dots represent hydrographic sites compiled in the GLODAP dataset [*Key et al.*, 2004] with complete CO_2 system variables (T, S, P, Si, ALK, TCO_2, and anthropogenic CO_2) for spring and summer (March-September) and diamonds are two hydrographic sites (July) closest to core-tops in the Norwegian Sea. Triangles in regions B and C are hydrographic sites used in panels (b) and (c). The dashed curves represent the approximate position of the Polar Front during the LGM [*Pflaumann et al.*, 2003]. Map was generated using ODV [*Schlitzer*, 2006]. Summer pCO_2 depth profiles in (b) Labrador Sea in 1998 and (c) Irminger Sea in 1981 from the GLODAP data set [*Key et al.*, 2004]. The curves in Figures 1b and 1c represent approximate trends of seawater pCO_2 with increasing water depth. At 50 m water depth (horizontal grey bar), the in situ pCO_2 (vertical grey bars) at both locations are clearly higher than the surface pCO_2 (0 m water depth) during the summer season.

Table 1. Core-top *N. pachyderma* (s) B/Ca, Cd/Ca and $\delta^{11}B$, together with estimated habitat hydrographic data and calculated partition coefficients and $\delta^{11}B_{cc\text{-}B4}$.

		Hydrographic Data (50m water depth)				Foraminiferal Results						
Core	Lat., Long., Water Depth (°N, °W, m)	T (°C)	P (μmol/kg)	$B(OH)_4^-/HCO_3^-$ (mol/mol)	$\delta^{11}B_{B(OH)4-}$ (‰)	B/Ca (μmol/mol)	K_D (x1000)	Cd/Ca (μmol/mol)	D_{Cd}	$\delta^{11}B$ (‰)	$\delta^{11}B_{cc\text{-}B4}$ (‰)	^{14}C age (years)
South Iceland Basin												
RAPID24-13B	60.17, 39.12, 2748	6.41	0.740	0.0446	17.37	61.5	1.379	0.0429	2.83	13.80 ± 0.27	−3.57	2325 ± 37
RAPID24-13B	60.17, 39.12, 2748	6.41	0.740	0.0446	17.37					14.08 ± 0.27	−3.29	2325 ± 37
RAPID26-14B	59.58, 41.17, 2302	6.03	0.747	0.0440	17.32	63.4	1.441	0.0527	3.44			
Labrador Sea												
RAPID28-16B	58.65, 44.22, 1627	5.39	0.755	0.0427	17.22	61.6	1.442	0.0619	4.00			
RAPID29-18B	58.80, 44.86, 2145	5.24	0.752	0.0424	17.20	63.5	1.497	0.0624	4.04	14.20 ± 0.26	−3.00	2325 ± 37
RAPID31-21B	58.61, 46.91, 2570	4.76	0.751	0.0414	17.12	63.5	1.534	0.0482	3.13	13.61 ± 0.26	−3.51	3043 ± 35
RAPID32-22B	58.25, 47.01, 3096	4.68	0.755	0.0413	17.11	61.1	1.481	0.0375	2.42	13.85 ± 0.26	−3.26	1084 ± 37
RAPID33-23B	57.94, 46.51, 3016	4.75	0.760	0.0415	17.13	62.9	1.517	0.0505	3.24	13.33 ± 0.27	−3.80	1426 ± 37
RAPID34-24B	57.59, 48.51, 3496	4.13	0.764	0.0404	17.04	61.6	1.527	0.0454	2.89	13.42 ± 0.28	−3.62	927 ± 37
RAPID35-25B	57.51, 48.72, 3486	4.05	0.765	0.0402	17.03	56.5	1.403	0.0555	3.53	14.33 ± 0.27	−2.70	582 ± 37
RAPID37-26B	54.51, 52.95, 1380	1.68	0.825	0.0382	16.86	56.4	1.475	0.0355	2.07			300 ± 38
RAPID38-27B	54.53, 52.43, 2152	1.81	0.823	0.0384	16.88	59.0	1.536	0.0383	2.24	13.19 ± 0.30	−3.69	328 ± 37
RAPID39-28B	54.91, 51.48, 2863	2.19	0.814	0.0388	16.91	63.9	1.650	0.0319	1.89			625 ± 35
RAPID40-29B	50.96, 49.96, 1044	3.42	0.711	0.0414	17.18	60.9	1.472	0.0362	2.50			436 ± 37
RAPID41-30B	50.71, 49.71, 1271	3.81	0.686	0.0417	17.21	62.5	1.496	0.0439	3.15			1128 ± 37
Norwegian Sea												
GS06-144-15MCA[a]	62.86, 6.11, 592	4.80	0.640	0.0443	17.34	67.1	1.513	0.0317	2.46			recent
GS06-144-16MCA[a]	62.84, 6.17, 550	4.80	0.640	0.0443	17.34	65.8	1.485	0.0358	2.78			recent
GS06-144-19MCA[a]	63.76, −5.19, 922	5.70	0.470	0.0500	17.88	66.0	1.319	0.0304	3.30			recent

[a]Habitat depths (55 m at 15 MCA and 16MCA, and 35 m at 19MCA) are assigned at $\sigma_t = 27.65$ kg/m^3, according to *Simstich et al.* [2003].

measurements. The chronology of these cores is from *Thornalley et al*. [2010]. The sedimentation rates for the two cores are 10–50 cm/1000 years during the last deglacial period. These cores are bathed in deep waters supersaturated with respect to calcite [*Yu et al*., 2010], and therefore dissolution of foraminiferal tests is minimal.

[11] Approximately, 100–200 tests (~1 mg) of *N. pachyderma* (s) were picked from the 150–250 μm size fraction and then cleaned following the "Mg-cleaning" procedure [*Barker et al*., 2003]. Analysis of trace element concentrations followed the method described in *Yu et al*. [2005]. The long-term relative precisions (2σ) for B/Ca and Cd/Ca are 5.2% and 10% based on duplicate measurements of in-house standards with B/Ca = 150 μmol/mol (n = 638, 1SD = 3.9 μmol/mol) and Cd/Ca = 0.024 μmol/mol (n = 233, 1SD = 0.001 μmol/mol), respectively.

[12] A comparison of different cleaning methods showed little effect on foraminiferal B/Ca [*Yu and Elderfield*, 2007]. Although previous studies on foraminiferal Cd/Ca have typically used reductive cleaning [*Boyle and Keigwin*, 1985/86], we employed the "Mg-cleaning" method [*Barker et al*., 2003] for both core-top and down-core samples. We do so for the following reasons: (i) *Yu et al*. [2007a] discovered a significant decrease in benthic foraminiferal Cd/Ca in core-tops during the reductive cleaning step in the laboratory. The decreases are not caused by hydrazine, the reagent originally employed to remove Fe-Mn oxides [*Boyle and Keigwin*, 1985/86], but are due to dissolution of carbonates by citrate [*Yu et al*., 2007a]. A similar phenomenon has also been observed for planktonic foraminifera [*Bian and Martin*, 2010]. Due to the very low Mn/Ca of these samples (down to ~2 μmol/mol, even without reductive cleaning) [*Bian and Martin*, 2010], decreases in Cd/Ca are unlikely to be caused by removal of any Mn coatings and are more likely due to preferential leaching of Cd from foraminiferal carbonate or dissolution of high-Cd carbonate phases [*Yu et al*., 2007a], although we acknowledge that further work is necessary to pin down the exact reasons. (ii) Mn/Ca values for core-top samples are <20 μmol/mol, well below the generally accepted threshold of 100 μmol/mol [*Boyle*, 1983], suggesting the absence of, or minimal, coatings associated with these samples. (iii) No correlation is observed between Cd/Ca and Mn/Ca (Fe/Ca) for our two down-core records, either separately or combined together ($r < 0.1$, $P > 0.28$) (Figures 2 and S1 in the auxiliary material). Down-core samples at deeper depths generally show higher Mn/Ca and Fe/Ca ratios. These increasing trends in Mn/Ca and Fe/Ca are in stark contrast to decreasing Cd/Ca down-core. One would expect to observe increasing Cd/Ca down-core and positive correlations with Mn/Ca and Fe/Ca, were Cd from Fe-Mn-containing coatings significant. (iv) The two down-cores show consistent Cd/Ca ratios, despite their different Mn/Ca ranges of 21–285 μmol/mol for 1P and 108–495 μmol/mol for 4P and very large contrast in Mn/Ca up to ~300 μmol/mol at some time intervals (Figure 2), which may be associated with various degrees of diagenesis in sediments under different sedimentation environments at different water depths (1P: 1237 m; 4P: 2133 m). Similarly, large Fe/Ca ratios are observed between the two cores. These provide strong evidence for insignificant contribution of Cd from Fe-Mn coatings [*Boyle*, 1983], if any, in our core sites. (v) At 10.5–12 ka and 15.2–16.1 ka (Figure 2), Mn/Ca in 1P are below the commonly used threshold of 100 μmol/mol and one would expect Cd/Ca from these time intervals are not significantly compromised by Mn coatings [*Boyle*, 1983]. Over the same time intervals, Mn/Ca in 4P range from 174 to 332 μmol/mol but Cd/Ca in 4P are similar to those from 1P, implying that Mn coatings are Cd-absent or Cd-depleted in our cores. (vi) Our Cd/Ca are fully consistent with a low resolution Cd/Ca in *N. pachyderma* (s), cleaned by the full reductive cleaning protocol [*Boyle and Keigwin*, 1985/86], for a nearby core NEAP 4K (61.5°N, 24.2°W, 1627 m; Figure 2b) [*Rickaby and Elderfield*, 2005], confirming that our Cd/Ca data are not contaminated by any Fe-Mn coating contamination. (vii) We use the same cleaning method for both our core-top and down-core samples, for consistency in this paper. Based on the above, we assert that it is unlikely that our Cd/Ca are compromised by the influence of any Fe-Mn coating contamination due to the exclusion of the reductive cleaning step. Instead, our results suggest that high Mn/Ca and Fe/Ca ratios do not necessarily indicate Cd contamination from Fe-Mn coatings at all times. We recommend that a comparison of Cd/Ca in shells from adjacent cores, bathed in the same water masses but experienced different diagenesis histories, could provide a useful approach to evaluate influences from Fe-Mn coatings. Possible cleaning effects on foraminiferal Cd/Ca may vary for samples from different environments and further studies are warranted in the future.

[13] The $\delta^{11}B$ ratios were measured on a Neptune MC-ICP-MS according to the method of *Foster* [2008] with an average uncertainty (2SD external reproducibility equivalent) of ±0.25‰ [*Foster*, 2008; *Rae et al*., 2011]. Each sample for $\delta^{11}B$ had ~400–700 shells (equivalent to ~3–5 mg) from the 150–250 μm size fraction and was also cleaned following the "Mg-cleaning" procedure [*Barker et al*., 2003]. Because of large sample size requirements, significantly more laboratory effort, and the availability of shells, we measured $\delta^{11}B$ for only eight samples from core-tops and seven samples down-core. Foraminiferal Mg/Ca and $\delta^{18}O$ are from *Thornalley et al*. [2011b].

[14] Hydrographic variables used in our core top calibration are estimated from nearby Global Ocean Data Analysis Project (GLODAP) sites [*Key et al*., 2004]. For sites in the South Iceland Basin and Labrador Sea, we estimate hydrographic conditions at a habitat depth of 50 m and between March and September, as a nearby sediment trap study in the Irminger Sea shows that spring and late summer blooms account for >95% of the total annual flux in the 150–250 μm size fraction [*Jonkers et al*., 2010]. In the Norwegian Sea, *N. pachyderma* (s) shows a single blooming during the summer at water depths with a constant density of σ_t = ~27.65 kg/m^3 [*Simstich et al*., 2003]. Water depths with σ_t = 27.65 kg/m^3 correspond to 55 m at core-top sites GS06-144-15MCA/16MCA, and 35 m at site GS06-144-19MCA (Table 1). Owing to the paucity of hydrographic sites, we used the two closest hydrographic sites (July) available in GLODAP to estimate seawater $[B(OH)_4^-/HCO_3^-]$ and $\delta^{11}B$ of $B(OH)_4^-$ for three core-tops from the Norwegian Sea, which could introduce large uncertainties. However, we stress that exclusion of Norwegian Sea core-tops from our calibration does not affect our conclusions.

[15] Hydrographic conditions at the habitat depth of *N. pachyderma* (s) at our core sites were interpolated from GLODAP data using the 3-D estimation function in Ocean

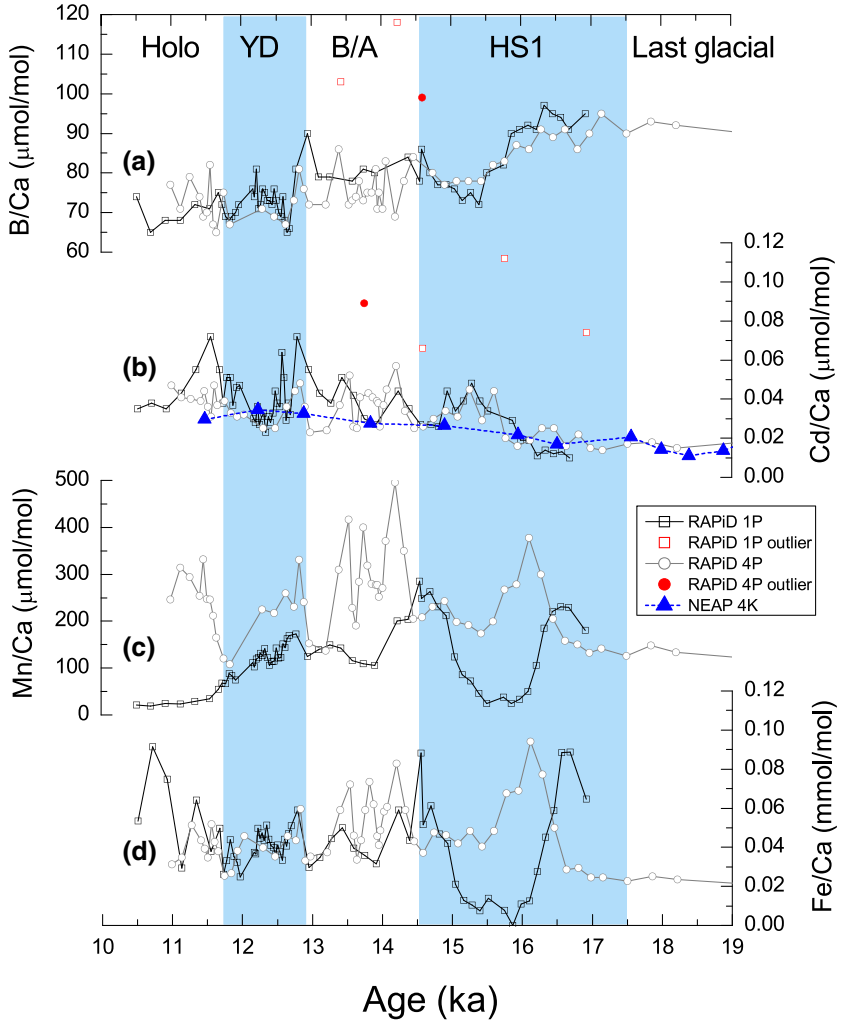

Figure 2. Comparison of *N. pachyderma* (s) (a) B/Ca, (b) Cd/Ca, (c) Mn/Ca, and (d) Fe/Ca ratios from two nearby cores RAPiD 1P and 4P from the polar North Atlantic (Figure 1a). Also shown in Figure 2b is Cd/Ca in *N. pachyderma* (s), cleaned by full reductive cleaning protocol [*Boyle and Keigwin*, 1985/86], from a nearby core NEPA 4K (61.5°N, 24.2°W, 1627 m) [*Rickaby and Elderfield*, 2005]. Despite their distinctive trends in Mn/Ca and Fe/Ca, the two cores show consistent B/Ca and Cd/Ca ratios, and have absolute Cd/Ca comparable to reductively cleaned samples from an adjacent core NEAP 4K. There is no correlation between B/Ca and Mn/Ca (Fe/Ca) or between Cd/Ca and Mn/Ca (Fe/Ca) (Figure S1). Red discrete symbols are outliers. It is possible to contaminate one trace element without affecting others. In total, three B/Ca and four Cd/Ca outliers from the two cores are excluded, possibly due to laboratory contaminations. Holo: Holocene; YD: Younger Dryas; B/A: Bølling/Allerød, HS1: Heinrich Stadial 1.

Data View (ODV) [*Schlitzer*, 2006]. We only select hydrographic sites which have the complete set of variables used in CO_2 system calculations (i.e., sites with all T, S, P, Si, TCO_2, ALK, and anthropogenic CO_2; Figure 1a), as calculated $[B(OH)_4^-/HCO_3^-]$ may be biased if sites containing complete CO_2 variables are combined with those having only some of these variables. The only exception to this is for anthropogenic CO_2 data in the Norwegian Sea: no anthropogenic CO_2 estimates are available at these two sites, and so we assumed a constant value of 45 μmol/kg (the value observed for hydrographic sites in the Labrador Sea [*Key et al.*, 2004]) for 0–100 m in the water column. The anthropogenic CO_2 contribution was subtracted from TCO_2, and pre-industrial seawater $[B(OH)_4^-/HCO_3^-]$ are calculated using CO_2sys.xls (Ver. 12) [*Pelletier et al.*, 2005]. The equilibrium constants K_1 and K_2 are those from *Mehrbach et al.* [1973], refit by *Dickson and Millero* [1987], K_B according to *Department of Energy* (*DOE*) [1994]], K_{SO4} is from *Dickson* [1990], and we use the recently redetermined total boron value of *Lee et al.* [2010]. Core-top results are reported in Table 1 and down-core results are tabulated in the auxiliary material.

4. Core-Top Data

[16] The *N. pachyderma* (s) from core-top samples shows B/Ca ratios ranging from 56 to 67 μmol/mol (Figure 3a), similar to those observed in this species from the Southern Ocean [*Hendry et al.*, 2009]. Comparison of B/Ca ratios with seawater $[B(OH)_4^-/HCO_3^-]$ shows that B/Ca and seawater

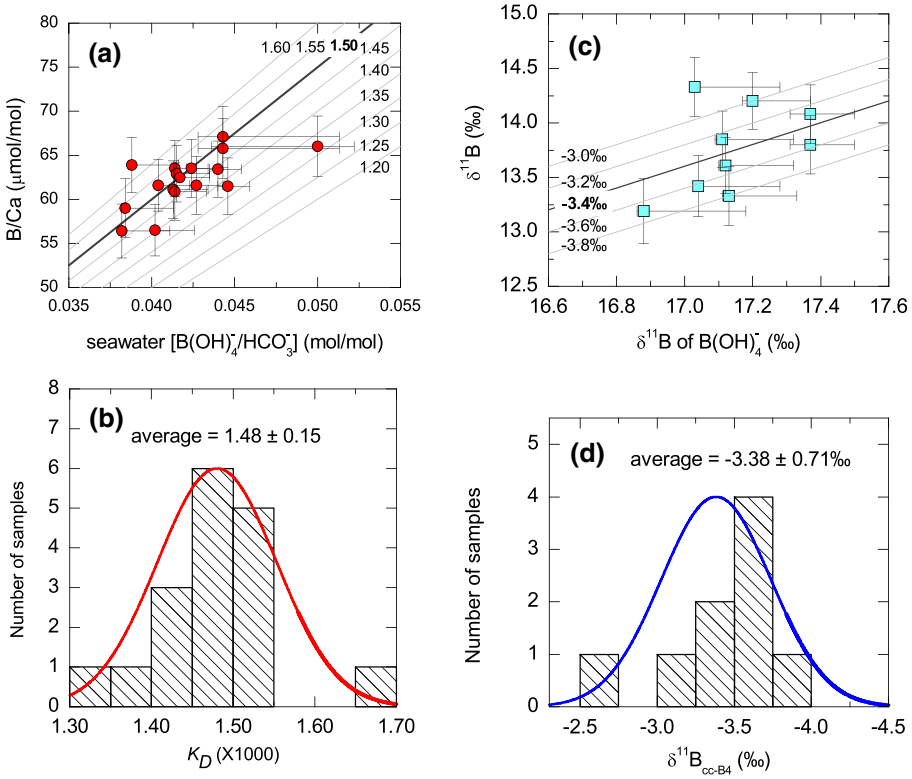

Figure 3. Core-top results for *N. pachyderma* (s). (a) B/Ca versus pre-industrial seawater $[B(OH)_4^-/HCO_3^-]$. Grey lines display values of K_D. (b) The histogram of calculated K_D with the normal distribution fit, showing a median value of $1.48 \pm 0.15 \times 10^{-3}$ (2σ). (c) *N. pachyderma* (s) $\delta^{11}B$ versus $\delta^{11}B$ of seawater $B(OH)_4^-$. Grey lines display values of $\delta^{11}B_{cc\text{-}B4}$. (d) The histogram of $\delta^{11}B_{cc\text{-}B4}$ with the normal distribution fit, showing a median value of 3.38 ± 0.71‰ (2σ). In Figures 3a and 3c, the *y* error bars are 2σ analytical uncertainty, whereas *x* error bars represent differences of hydrographic values at 40 m (+error) and 60 m (−error) from those at 50 m water depth.

$[B(OH)_4^-/HCO_3^-]$ are positively correlated ($r = 0.66$, $P < 0.0001$) and K_D into *N. pachyderma* (s) is normally distributed with a mean of $1.48 \pm 0.15 \times 10^{-3}$ (2σ) (Figures 3a and 3b).

[17] Core-top *N. pachyderma* (s) $\delta^{11}B$ displays a range of 13.19–14.33‰, significantly lower than the estimated $\delta^{11}B$ of seawater $B(OH)_4^-$ of 16.88–17.37‰ at these sites (Table 1 and Figures 3c and 3d). The $\delta^{11}B$ offset between shell carbonate and seawater $B(OH)_4^-$, $\delta^{11}B_{cc\text{-}B4}$, shows a range of −2.7‰ to −3.8‰ with an average of -3.38 ± 0.71‰ (2σ). Negative $\delta^{11}B_{cc\text{-}B4}$ offsets as seen in *N. pachyderma* (s) have previously been observed in another symbiont-barren planktonic foraminifera *Neogloboquadrina dutertrei* ($\delta^{11}B_{cc\text{-}B4} \approx -1.5$‰), and contrast with the positive $\delta^{11}B_{cc\text{-}B4}$ offsets associated with symbiont-bearing species *G. ruber* and *G. sacculifer* [*Foster*, 2008]. $\delta^{11}B_{cc\text{-}B4}$ offsets have previously been attributed to incorporation of boric acid (which has $\delta^{11}B \sim 27$‰ higher than borate), pH elevation during calcification, or alteration of microenvironment pH by CO_2 released during foraminifera and symbiont respiration, or CO_2 taken up by symbiont photosynthesis [e.g., *Foster*, 2008; *Hönisch et al.*, 2003; *Klochko et al.*, 2009; *Zeebe et al.*, 2003]. The negative offsets we observe in *N. pachyderma* (s) cannot be simply related to boric acid incorporation, nor to pH elevation during calcification, both of which would raise foraminifera $\delta^{11}B$ above that of seawater borate. One explanation for these offsets, which is applicable to all the species mentioned above, is alteration of the foraminiferal microenvironment by respiration and photosynthesis [e.g., *Hönisch et al.*, 2003; *Zeebe et al.*, 2003]. This may cause negative $\delta^{11}B_{cc\text{-}B4}$ in the symbiont-barren species due to respiration and positive $\delta^{11}B_{cc\text{-}B4}$ in the symbiont-bearing species due to photosynthesis. Alternatively, the offset may be due to some unknown vital effects. As with previous studies [e.g., *Foster*, 2008; *Zeebe et al.*, 2003], this offset is assumed to be constant.

[18] To explore possible links between upper ocean pCO_2 and nutrients in the past, we use *N. pachyderma* (s) Cd/Ca ratios to reconstruct past subsurface water P contents, following the approach described by *Rickaby and Elderfield* [1999]. We use core-top Cd/Ca data to define a partition coefficient between *N. pachyderma* (s) calcite and seawater Cd (D_{Cd}) appropriate for our sites. Seawater P and temperature were estimated using the same approach as for B/Ca calibration, except that we used all hydrographic sites with P and T during the spring-summer season rather than only selecting sites with all the carbonate system parameters. Seawater P is related to seawater Cd using $Cd = Cd^t/[\alpha \times (P^t/P - 1) + 1]$, where $Cd^t = 1.2$ nmol/kg, $P^t = 3.3$ μmol/kg, and $\alpha = 2$ from *Elderfield and Rickaby* [2000]. A constant Ca concentration of 0.01 mol/kg is used to calculate seawater Cd/Ca. Then the partition coefficient of Cd into calcite of *N. pachyderma* (s) is obtained from $D_{Cd} = (Cd/Ca)_{foram}/(Cd/Ca)_{sw}$. Similar to what

is observed for *G. bulloides* [*Rickaby and Elderfield*, 1999], D_{Cd} for *N. pachyderma* (s) shows an exponential dependence on the calcification temperature (Figure 4).

5. Variability of K_D and $\delta^{11}B_{cc\text{-}B4}$ and Complications with Core-Top Calibrations

[19] We observe considerable variability in K_D and $\delta^{11}B_{cc\text{-}B4}$ associated with core-top *N. pachyderma* (s) (Figure 3), which is significantly greater than our analytical uncertainties and may be largely due to weak constraints related to paucity of our hydrographic data. As can be seen in Figure 1a, suitable hydrographic sites in this region are sparse and are from a limited number of cruises (in 1981, 1997, and 1998) [*Key et al.*, 2004], especially for the Norwegian Sea samples. This inevitably introduces errors in estimates of hydrographic conditions for core-top shell samples which likely represent the average carbonate system conditions over many years. It is probably an oversimplification to use an average habitat depth for calibration. The calcification depth of *N. pachyderma* (s) may vary significantly in different ocean regions. For example, this species has been found to live at depths varying between ~30 m and 250 m in the Arctic and Nordic Seas [e.g., *Bauch et al.*, 1997; *Hillaire-Marcel and de Vernal*, 2008; *Nyland et al.*, 2006; *Simstich et al.*, 2003]. *N. pachyderma* (s) also migrates vertically in the water column through its life cycle, experiences encrustation, and cements secondary calcites at depth [e.g., *Simstich et al.*, 2003]. Error bars in Figure 3 show the influences from potential changes in the habitat depth between 40 and 60 m. At the depth of the thermocline where large gradients in seawater pCO_2 occur (Figures 1b and 1c), even a small variation in water depth (especially to shallow depths) is accompanied with large changes in seawater $[B(OH)_4^-/HCO_3^-]$ and $\delta^{11}B$ of $B(OH)_4^-$ (Figure 3). Furthermore, the blooming season of this species may vary [*Kuroyanagi et al.*, 2011]. In addition, our core-top samples are from locations that span relatively narrow ranges in seawater $[B(OH)_4^-/HCO_3^-]$ and $\delta^{11}B$. We cannot include *N. pachyderma* (s) B/Ca data from the Southern Ocean [*Hendry et al.*, 2009] in our calibration, because there is no seawater $[B(OH)_4^-/HCO_3^-]$ for those samples. We encourage high-quality core-top samples from other regions with sufficiently different carbonate chemistry to extend the calibration (Figure 3).

[20] The range of ages characterizing our core-tops and the change in atmospheric CO_2 during this period may also add to the observed variability. Although our core-top samples are from relatively high sedimentation rate box cores, radiocarbon dates show an age range of 0 to ~3000 years (conventional radiocarbon age) (Table 1 and Figure 5). *N. pachyderma* (s) B/Ca shows a significant decrease since industrialization, mirroring the rising atmospheric CO_2 (Figure 5); only one $\delta^{11}B$ measurement falls within this period

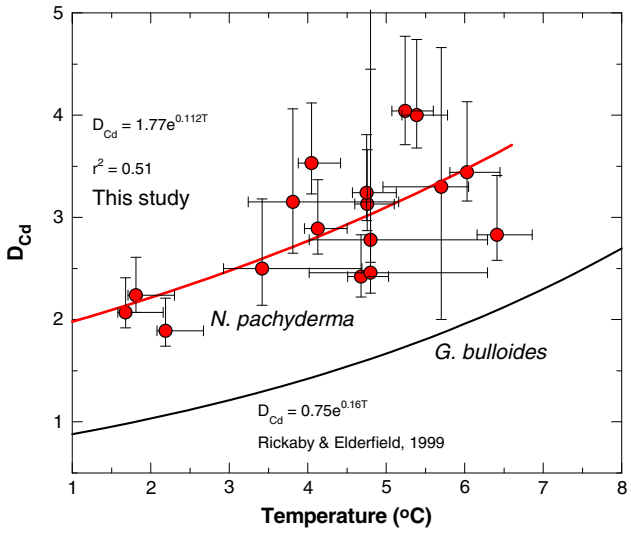

Figure 4. Calibration of D_{Cd} and temperature for *N. pachyderma* (s) using core-top samples. The calibration for *G. bulloides* is shown for comparison (original in [*Rickaby and Elderfield*, 1999] and subsequently revised in [*Elderfield and Rickaby*, 2000]). The error bars represent differences in D_{Cd} and temperature using hydrographic values at 40 m (+error) and 60 m (−error) from those at 50 m water depth.

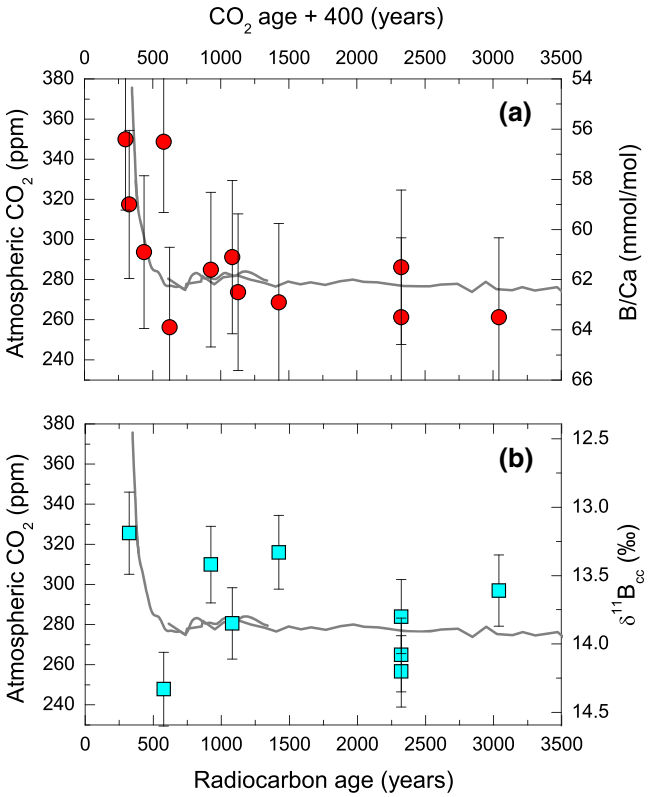

Figure 5. Comparison of *N. pachyderma* (s) (a) B/Ca and (b) $\delta^{11}B$ (B) from RAPiD core-tops (Table 1) with atmospheric CO_2. Atmospheric CO_2 records (curves) are from Vostok [*Monnin et al.*, 2001], Law Dome [*Etheridge et al.*, 1996], and Mauna Loa [*Keeling et al.*, 2004]. The ages of atmospheric CO_2 are shifted 400 years older to account for the reservoir age effect in the North Atlantic following [*Broecker et al.*, 1990], so that they can be directly compared with core-top samples. Note the decreasing values in B/Ca, and possibly $\delta^{11}B$, as atmospheric CO_2 rose abruptly since industrialization. The juxtaposition of ordinate scales is arbitrary and the *y* axes of B/Ca and $\delta^{11}B$ and atmospheric CO_2 are not scaled by any relationship.

and also shows a slight decrease. Due to low temperatures and relatively low TCO_2, surface water CO_2 content in the North Atlantic is highly sensitive to atmospheric CO_2 increases [*Feely et al*., 2004]. With increasing atmospheric CO_2, surface water pH, $[B(OH)_4^-/HCO_3^-]$, and $\delta^{11}B$ of $B(OH)_4^-$ will decrease. Thus, it is inappropriate to use pre-industrial CO_2 values to calculate K_D for very young core-tops ($\lesssim$500 years radiocarbon age). If we use modern TCO_2 (measured in June 1998, the only cruise available in GLODAP) [*Key et al*., 2004] for these young samples, the calculated K_D would be ~$1.79–1.87 \times 10^{-3}$ and $\delta^{11}B_{cc\text{-}B4}$ would be approximately −2.95‰, slightly higher than the averages using all core-tops (Table 1 and Figure 3). However, the hydrographic data (mainly TCO_2) from this single cruise are unlikely to accurately represent the conditions over the time interval when these core-top shells calcified (presumably a few decades to a hundred years), in the face of a very rapid rise in atmospheric CO_2 during the past century (Figure 5).

[21] Altogether, the above factors would contribute to K_D and $\delta^{11}B_{cc\text{-}B4}$ variations observed in our core-top samples. It is a problem that will beset all such calibration attempts given the timescale mismatch between sediment and water data. However, core-top samples serve as the closest analogue to down-core samples as they both have calcified in natural marine environments and experienced various processes including growth at surface, secondary encrustation during vertical migration in the water column, and subsequent burial in sediments. The calibrations in Figure 3 represent our best estimates based on currently available hydrographic data and our understanding about the habitat of *N. pachyderma* (s) in the North Atlantic. Below, we assumed constant K_D of 1.48×10^{-3} and $\delta^{11}B_{cc\text{-}B4}$ of −3.38‰ for our down-core calculations. We strongly encourage further studies such as laboratory culturing [e.g., *Allen et al*., 2011] and plankton tows combined with simultaneous measurements of hydrographic data to improve our understanding about boron incorporation into *N. pachyderma* (s).

[22] When applying *N. pachyderma* (s)-based proxies to down-core data, we must bear in mind the uncertainty in assigning a specific depth habitat for *N. pachyderma* (s). Our down-core proxy data should therefore be interpreted simply in terms of our best estimate of past subsurface pCO_2. However, because surface pCO_2 at 0 m water depth is always lower than at greater depths (Figures 1b and 1c), our subsurface pCO_2 reconstructions also provide a constraint for the maximum possible value of surface pCO_2. As will be shown, our subsurface pCO_2 reconstructions are lower than atmospheric pCO_2, enabling us to suggest that the polar North Atlantic has remained a CO_2 sink during the calcification seasons of *N. pachyderma* (s) over the last deglaciation.

6. Down-Core Data

[23] The *N. pachyderma* (s) from 1P and 4P shows a similar trend and a comparable range in B/Ca of 64–97 μmol/mol during the last deglacial period (Figure 6a). B/Ca ratios decreased by ~45% since the last glacial. The higher glacial B/Ca cannot be explained by an ~3% increase in seawater B concentration caused by ice growth during the glacial period (note the incorporation of boron into calcite does not involve Ca^{2+} according to equations (1) and (3)). The decrease of B/Ca during the last deglacial is not linear, displaying rapid decreases in B/Ca from 97 to 77 μmol/mol during Heinrich Stadial 1 (HS1) and from 77 to 64 μmol/mol during the Younger Dryas (YD), interrupted by a plateau during the Bølling/Allerød (B/A). This temporal change in *N. pachyderma* (s)B/Ca roughly mirrors that of atmospheric CO_2 (Figure 6d) [*Monnin et al*., 2001]. From the last glacial to early Holocene, *N. pachyderma* (s) $\delta^{11}B$ decreased from 16.25‰ to 14.84‰ (a change of −1.41‰) and followed the B/Ca trend (Figure 6a).

[24] We used a constant K_D of 1.48×10^{-3} (Figure 3b) to calculate past seawater $[B(OH)_4^-/HCO_3^-]$ from *N. pachyderma* (s) B/Ca (Figure 6a). In this case, any reconstructed changes in pH and pCO_2 should be driven by changes in B/Ca, not by K_D [*Allen and Hönisch*, 2012] (Figure S2). In addition to seawater $[B(OH)_4^-/HCO_3^-]$, a second variable is needed to fully constrain the seawater CO_2 system, and ALK is often used. The history of seawater ALK is poorly constrained and here we follow the previous approach of *Foster* [2008]. We estimate surface seawater ALK in which *N. pachyderma* (s) calcified using the equation of $ALK = 2305 + 53.97 \times (S - 35) + 2.74 \times (S - 35)^2 - 1.16 \times (T - 20) - 0.040 \times (T - 20)^2$ from *Lee et al*. [2006], assuming that this relationship has remained unchanged since the last glacial maximum (Figure 7). However we note that given the close relationship between $[B(OH)_4^-/HCO_3^-]$, pH and $[CO_2]$, our pCO_2 estimates are mainly driven by our $\delta^{11}B$ and B/Ca data; in other words, a large uncertainty of ±3% or approximately ±100 μmol/kg for ALK (arbitrarily assigned, compared to approximately ±50 μmol/kg in *Palmer and Pearson* [2003]) produces relatively small errors in pCO_2 (Figure 6) [*Foster*, 2008; *Hönisch et al*., 2008; *Palmer and Pearson*, 2003]. Calcification temperatures for *N. pachyderma* (s) are reconstructed using $Mg/Ca(T_{Mg/Ca})$ [*Thornalley et al*., 2011b]. With *N. pachyderma* (s) $\delta^{18}O_{cc}$ and $T_{Mg/Ca}$, the seawater $\delta^{18}O_{sw}$ is calculated using the equation: $\delta^{18}O_{sw} = (\delta^{18}O_{cc} + 0.27) - [4.64 - (4.64^2 - 4 \times 0.09*(16.1 - T_{Mg/Ca}))^{0.5}]/(2 \times 0.09)$ [*Kim and O'Neil*, 1997]. To estimate salinity from $\delta^{18}O_{sw}$, rather than use the modern $S - \delta^{18}O_{sw}$ relationship which is unlikely to be robust during the deglaciation when meltwater input was high, we employ a simple mixing model, with a freshwater end-member $\delta^{18}O_{sw}$ value of −30‰, based on typical values for ice melt in this region [*Azetsu-Scott and Tan*, 1997; *Rasmussen et al*., 2006]. It is possible to use other models to calculate S (such as the modern Norwegian Sea $S - \delta^{18}O_{sw}$ relationship [*LeGrande and Schmidt*, 2006]), but these do not yield S values outside the estimated error assigned to S of 1‰ and would have little effect on the calculated pH, CO_3^{2-}, and pCO_2. Furthermore, while 1P and 4P showed very different S during the late HS1 (Figure 7c), which may be associated with more intense local surface freshening and/or brine rejection at 1P [*Thornalley et al*., 2011a; *Thornalley et al*., 2010], the two cores show very similar carbonate system and pCO_2 trends (Figures 6b–6d). This suggests that the B/Ca methodology is relatively insensitive to S changes. With $T_{Mg/Ca}$, S, ALK, and $[B(OH)_4^-/HCO_3^-]$, we calculate seawater pH, CO_3^{2-}, and pCO_2 (Figures 6b–6d) using CO_2sys.xls by iteration in Excel [*Pelletier et al*., 2005]. We applied a constant $\delta^{11}B_{cc\text{-}B4}$ of −3.38‰ (Figures 3c and 3d) to convert *N. pachyderma* (s) $\delta^{11}B$ to seawater pH using equation (2), and combined this with ALK, to obtain surface CO_3^{2-} and pCO_2, following the approach in *Foster* [2008] (Figure 6). Error

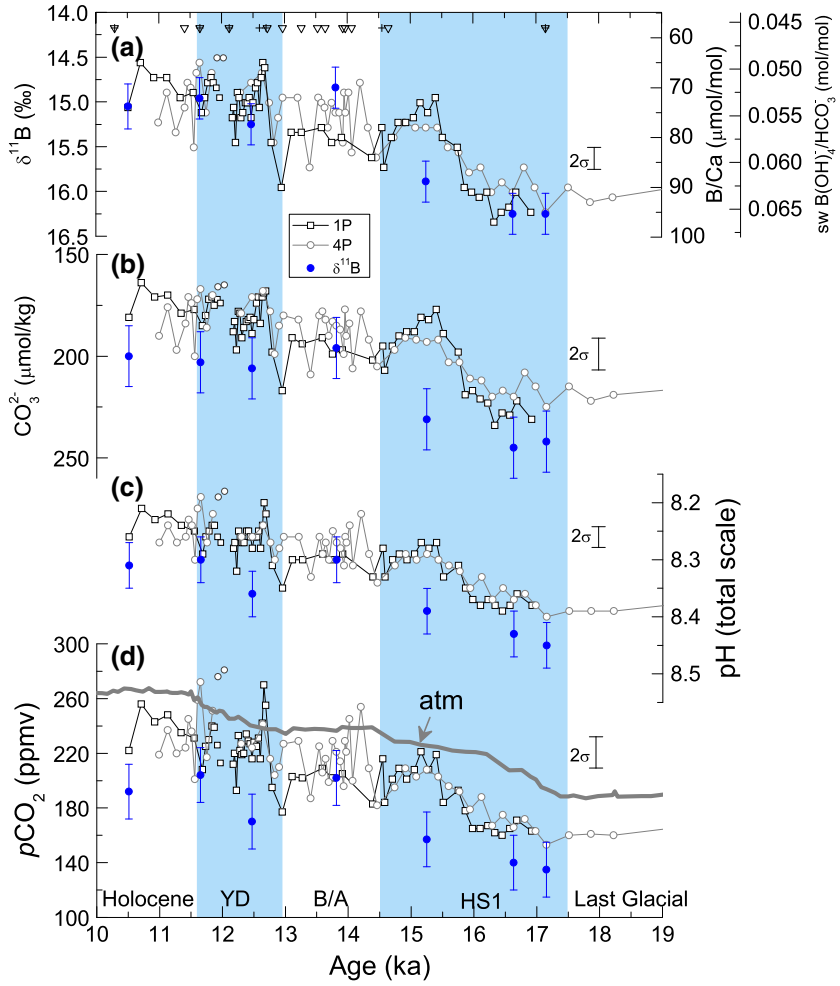

Figure 6. Deglacial records of *N. pachyderma* (s) B/Ca and (a) $\delta^{11}B$, (b) reconstructed subsurface water CO_3^{2-}, (c) pH, and (d) pCO_2 for two nearby cores 1P and 4P off Iceland. Error bars indicate average 2σ uncertainties, fully propagated from individual errors associated with $T_{Mg/Ca}$ (±1.5°C, corresponding to ±0.02 units in pH, ±2 μmol/kg in CO_3^{2-}, and ±12 ppmv in pCO_2), S (±1‰, corresponding to ±0.02 units in pH, ±3 μmol/kg in CO_3^{2-}, and ±9 ppmv in pCO_2), ALK (±3%, corresponding to ±0.01 units in pH, ±11 μmol/kg in CO_3^{2-}, and ±7 ppmv in pCO_2), B/Ca (±5.2%, corresponding to ±0.03 units in pH, ±8 μmol/kg in CO_3^{2-}, and ±14 ppmv in pCO_2), and $\delta^{11}B$ (±0.25‰, corresponding to ±0.02 units in pH, ±8 μmol/kg in CO_3^{2-}, and ±12 ppmv in pCO_2). Symbols along the upper *x* axis (triangles, 4P; crosses, 1P) in Figure 6a indicate age control points [*Thornalley et al.*, 2011a]. Atmospheric CO_2 in Figure 6d is from [*Monnin et al.*, 2001] plotted against the age model from *Lemieux-Dudon et al.* [2010]. Four discrete solid symbols from 11.92–12.03 ka denote samples that may be affected by turbidites.

sourced from individual input variables is given in Figure 6. The average integrated reconstruction uncertainties for B/Ca and $\delta^{11}B$ are similar, at ±0.04 units in pH, ±15 μmol/kg in CO_3^{2-}, and ±20 ppmv in pCO_2 (2σ), respectively.

7. Comparison of CO_2 Variables Derived from B/Ca and $\delta^{11}B$

[25] As *N. pachyderma* (s) B/Ca and $\delta^{11}B$ were measured in shells from the same depths, they should yield similar pH, CO_3^{2-}, and pCO_2 values, if the K_D and $\delta^{11}B_{cc\text{-}B4}$ values obtained from core-top samples are correct. All seawater pH, CO_3^{2-}, and pCO_2 values from B/Ca and $\delta^{11}B$ agree within their reconstruction uncertainties, though $\delta^{11}B$-based values mainly (five out of seven cases) lie below those from B/Ca (Figure 6). This suggests a systematic offset that could be removed with only a slight adjustment of K_D and/or $\delta^{11}B_{cc\text{-}B4}$. For example, if the $\delta^{11}B_{cc\text{-}B4}$ is adjusted from −3.38‰ to −3.1‰, which is still within the range of $\delta^{11}B_{cc\text{-}B4}$ (Figure 3d), $\delta^{11}B$-derived pH, CO_3^{2-}, and pCO_2 would entirely match those from B/Ca.

[26] Using a different habitat depth would shift both $\delta^{11}B$ and B/Ca derived values upward or downward in the same direction, with little effect on the temporal pattern (Figure S3). The discrepancy between B/Ca and $\delta^{11}B$-derived values becomes slightly larger down core, if 100 m habitat depth is chosen for the core-top calibration. This favors a shallow habitat depth for *N. pachyderma* (s). If we use a habitat depth of 30 m for core-tops, the down-core pH and pCO_2 results remain similar to those using 50 m habitat depth,

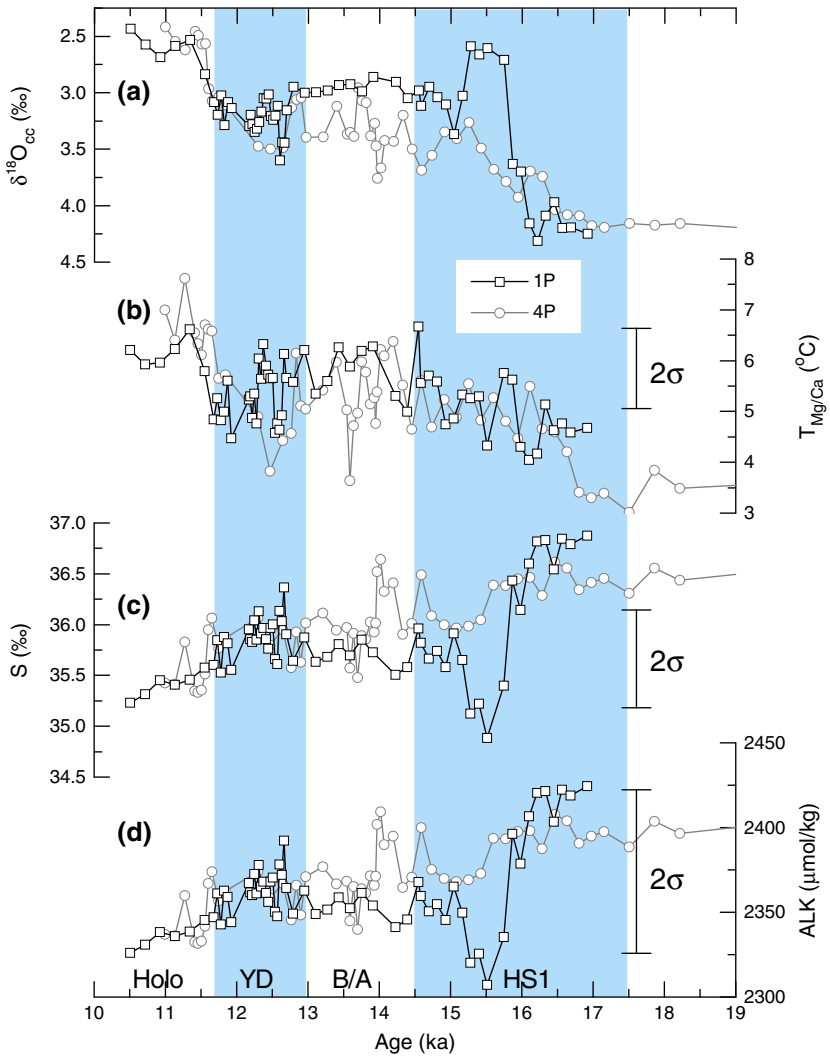

Figure 7. Derivation of seawater alkalinity (ALK) using salinity and temperature. (a) *N. pachyderma* (s) $\delta^{18}O$, (b) Mg/Ca derived calcification temperature ($T_{Mg/Ca}$) [*Thornalley et al.*, 2010], (c) salinity (S), and (d) seawater ALK based on the equation from *Lee et al.* [2006]. Error bars in Figures 7b–7d represent the average 2σ uncertainties of ±1.5°C in temperature, ±1‰ in salinity, and ±100 μmol/kg in ALK, respectively. It is worth noting that despite distinctive S and ALK histories at 1P and 4P, similar B/Ca at these two cores yield consistent pH and pCO_2 values (Figure 6d). This suggests that *N. pachyderma* (s) B/Ca methodology is not significantly affected by any salinity/ALK effect.

and the match of pH, CO_3^{2-}, and pCO_2 based on B/Ca and $\delta^{11}B$ does not improve compared to that using 50 m habitat depth (Figure S3).

[27] The slight mismatch in absolute estimates in pH, CO_3^{2-}, and pCO_2 from B/Ca and $\delta^{11}B$ cannot be attributed to secondary influences on K_D from seawater CO_3^{2-} or calcification temperature, because K_D in *N. pachyderma* (s) from core-tops and down-cores show no relationship with the calcification temperature or ambient CO_3^{2-} (Figure S4). At this time, we use constant K_D of 1.48×10^{-3} and $\delta^{11}B_{cc}$ of −3.38‰ in *N. pachyderma* (s) (Figure 3) for down-core reconstructions. Considering complications associated with our core-top calibrations (Section 5) as well as reconstruction uncertainties from the two independent methods, the agreement within uncertainty between the B/Ca and $\delta^{11}B$-based reconstructions is encouraging (Figure 6). We will show that using results from B/Ca and $\delta^{11}B$ independently would not affect our final conclusions regarding the CO_2 uptake history of the northern North Atlantic in the past.

8. Deglacial Subsurface pCO_2 Variation in the Northern North Atlantic

[28] Given its high temporal resolution, we focus on B/Ca derived pH, CO_3^{2-}, and pCO_2 in the discussion below. The last glacial (17.5–21 ka) to early Holocene (10.5–11 ka) changes in surface water pH, CO_3^{2-}, and pCO_2 at 1P and 4P are −0.13 units, −41 μmol/kg, and +70 ppmv, respectively (Figures 6b–6d). These changes are similar to those observed in the tropical and subtropical regions over the same time interval [*Foster*, 2008; *Hönisch and Hemming*, 2005; *Palmer and Pearson*, 2003; *Sanyal et al.*, 1997; *Yu et al.*, 2007b]. Our reconstructed subsurface pCO_2 is close to and generally follows the trend of atmospheric CO_2

[*Lemieux-Dudon et al.*, 2010; *Monnin et al.*, 2001], showing rapid rises during the HS1 and YD, interrupted by a pause during the B/A (Figure 6d). A few samples centered at 11.65, 12.66, and 14.20 ka showed pCO_2 values higher than the contemporary atmospheric CO_2. Typically, however, subsurface pCO_2 was lower than the contemporary atmospheric CO_2. During the last deglacial, the sea-air pCO_2 gradient (ΔpCO_2) between the habitat depth of *N. pachyderma* (s) and the atmosphere remained largely negative with an average value of -26 ± 35 ppmv (2σ variability of all data during the last deglacial) (Figure 8a), compared to the preindustrial offset of approximately -20 ppmv during spring-summer at 50 m water depth in this area [*Key et al.*, 2004; *Takahashi et al.*, 1993; *Takahashi et al.*, 2002].

[29] A close inspection of our pCO_2 and ΔpCO_2 records also reveals considerable millennial timescale variability (Figures 6d and 8a). For example, the ΔpCO_2 variability during the HS1, shown in both 1P and 4P, reached a maximum magnitude of ~40 ppmv between 15 and 16 ka. Changes in seawater pCO_2 off Iceland are affected by a combination of factors, including the pCO_2 of source waters from the Gulf Stream/North Atlantic Current and gradients in temperature, salinity/alkalinity, and nutrients from the source region to the core location. Reconstruction of surface

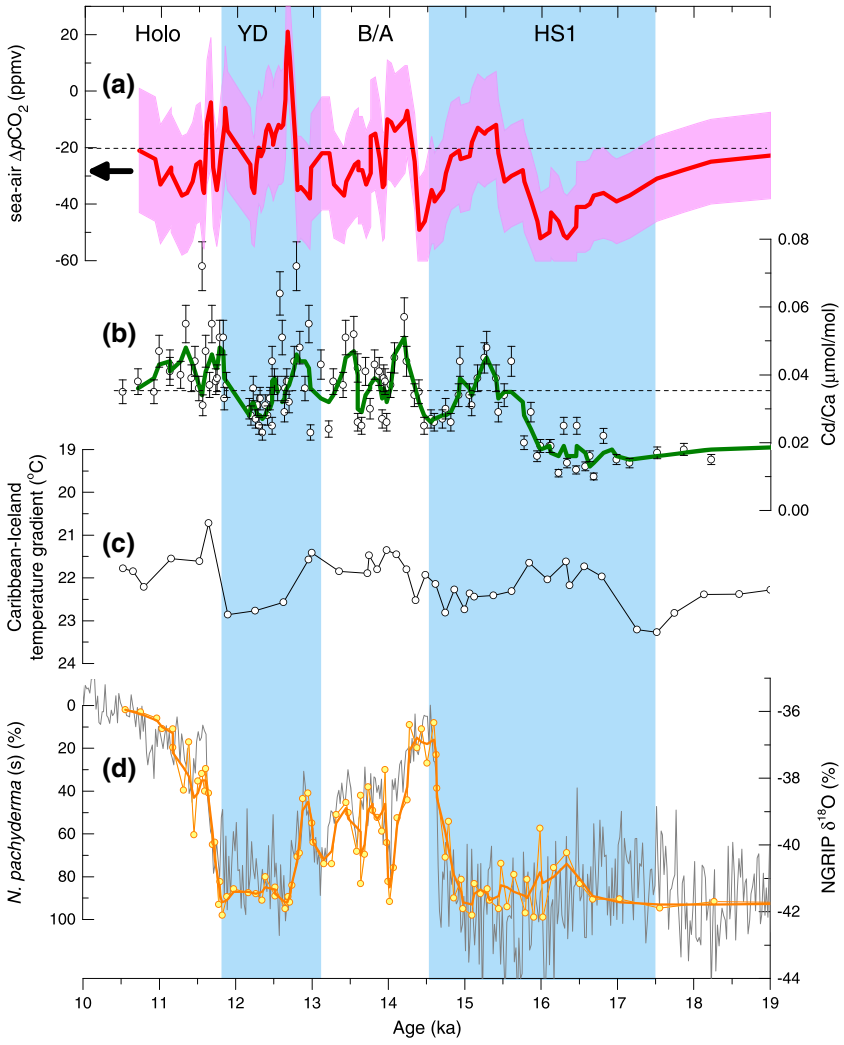

Figure 8. Comparison of deglacial sea-air ΔpCO_2 with other records from the North Atlantic. (a) Sea-air ΔpCO_2, calculated as the difference of contemporary subsurface water pCO_2 from *N. pachyderma* (s) and atmospheric pCO_2 as shown in Figure 6D. The solid curve is three-point running mean of the original ΔpCO_2 with the $\pm 2\sigma$ uncertainty envelope. The arrow represents the average ΔpCO_2 (-26 ± 35 ppmv) over the entire deglacial period, compared to the pre-industrial offset of ~ -20 ppmv at 50 m depth during the spring-summer season indicated by a dashed line [*Key et al.*, 2004]. (b) Variation in Cd/Ca in *N. pachyderma* (s). The solid curve represents the three-point running mean of the original data. Error bars represent $\pm 10\%$ (2σ) uncertainty. The horizontal dashed line represents the late Holocene value. Raw Cd/Ca shows almost exactly the same pattern as calculated P (Figure 9). (c) Mg/Ca temperature gradient between Caribbean Sea (ODP 999) [*Schmidt et al.*, 2004] and Iceland (1P/4P) [*Thornalley et al.*, 2011b]. (d) NGRIP $\delta^{18}O$ [*Rasmussen et al.*, 2006] and %*N. pachyderma* (s) for RAPiD 1P and 4P [*Thornalley et al.*, 2011b]. The orange curve without symbols represents three-point running mean.

water pCO_2 for core ODP 999 in the Caribbean Sea shows that surface water at low latitudes of the Atlantic has remained roughly in equilibrium with the atmosphere since the last glacial [*Foster*, 2008]. The temperature gradient between ODP 999 [*Schmidt et al.*, 2004] and 1P/4P [*Thornalley et al.*, 2011b] was only slightly greater (by <2°C) during the last glacial period than the early Holocene (Figure 8c) and shows no correlation with ΔpCO_2 (Figure 8a). These observations suggest that changes in source water pCO_2 and temperature gradients (ODP 999 versus 1P/4P) are not major reasons for past ΔpCO_2 variations observed at our sites.

[30] In contrast, similar trends are observed between ΔpCO_2 and the raw Cd/Ca (Figures 8a and 8b). We have used *N. pachyderma* (s) Mg/Ca derived $T_{Mg/Ca}$ to account for the temperature effect on D_{Cd}, based on the core-top calibration to reconstruct seawater P (Figures 4 and 9). Reconstructed seawater P and raw Cd/Ca are highly correlated (Figure 9D), suggesting that changes in down-core P are mainly caused by changes in Cd/Ca. Therefore, ΔpCO_2 and seawater P have covaried during the last deglaciation ($r = 0.46$, $P < 0.0001$, n = 114, all date from 19 to 10 ka; $r = 0.84$, $P < 0.0001$, n = 44, early deglacial from 17.5 to 14 ka; Figure S5). This covariation is not an artifact induced by (i) conversions from B/Ca to seawater pCO_2 because changes in pCO_2 are mainly driven by those in B/Ca, as reflected by the tight correlation between subsurface pCO_2 and B/Ca ($r^2 = 0.924$, $P < 0.0001$; Figure S2), or (ii) the age model uncertainty associated with our cores (Figure S6). A comparison of raw data suggests that the covariation between ΔpCO_2 and P is largely driven by the correlation between B/Ca and Cd/Ca (Figure S7). The covariation between ΔpCO_2 and P suggests that biological processes and/or mixing waters from above and below have played an important role in the observed variability of ΔpCO_2 (Figures 8a and 8b), as it does today [*Takahashi et al.*, 1993]. Using Redfield ratio stoichiometry and the Revelle factor to

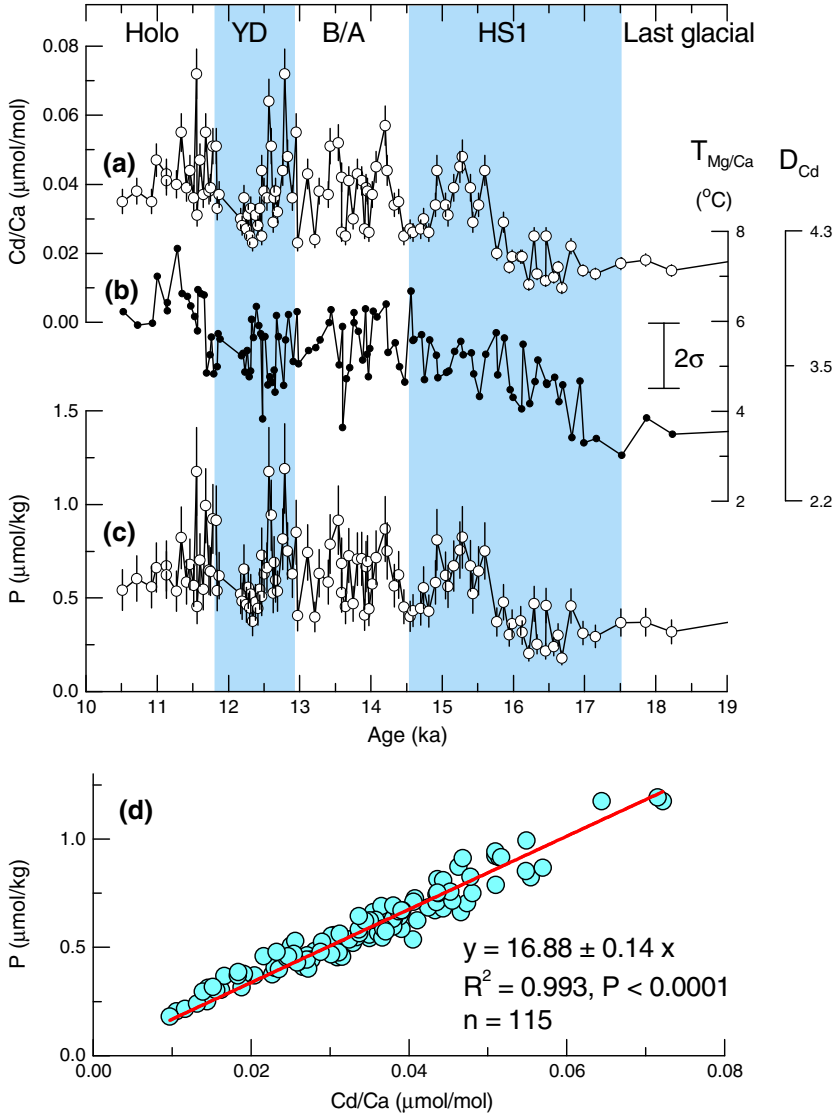

Figure 9. Down-core time series for (a) *N. pachyderma* (s) Cd/Ca, (b) D_{Cd} based on Mg/Ca temperature, and (c) reconstructed seawater P. Data from 1P and 4P are not separated here, as they show very similar trends. (d) Correlation between Cd/Ca and P.

estimate pCO_2 changes from our reconstructed seawater P change gives shifts in pCO_2 on the order of ~60 ppmv (Figure S5), supporting a significant control on ΔpCO_2 by changes in seawater nutrient concentration. The $\delta^{13}C$ of *N. pachyderma* (s) (Figure S8) may also be sensitive to changes in seawater nutrient content. However, it is likely that many additional factors affect planktonic $\delta^{13}C$, but not Cd/Ca [*Duplessy et al.*, 1988; *Kohfeld et al.*, 2000; *Lynch-Stieglitz et al.*, 1995], preventing an obvious correlation between Cd/Ca and $\delta^{13}C$.

9. The Role of the Polar North Atlantic in Atmospheric CO_2 During the Last Deglaciation

[31] Today, the polar North Atlantic serves as one of the major sinks of CO_2 in the global oceans [*Takahashi et al.*, 2002]. A change in the strength with which CO_2 is absorbed in the North Atlantic Ocean would influence atmospheric CO_2. The air-sea exchange of CO_2 is affected by sea-air ΔpCO_2 at 0 m water depth. Our reconstructed pCO_2 cannot be treated directly as past sea surface pCO_2, but represent values at the subsurface habitat depth (~50 m) of *N. pachyderma* (s) during the calcification seasons. However, subsurface pCO_2 is always higher than that at the surface due to regeneration of sinking biogenic matter and mixing with high-pCO_2 waters from deeper depths. Today, the offset in pCO_2 between 50 m and 0 m in the polar North Atlantic is about 40–90 ppmv during the summer (Figures 1b and 1c). If our application of a constant K_D from our core-top calibration is correct, the negative sea-air ΔpCO_2 based on *N. pachyderma* (s) indicates that even considering our reconstruction uncertainties of $\pm$20 ppmv, surface pCO_2 remained lower than contemporary atmospheric CO_2 during 19–10 ka. Therefore, like today, regions off Iceland in the polar North Atlantic served as a sink of CO_2 to the atmosphere during the calcification seasons of *N. pachyderma* (s) (spring to summer, if the modern observation in Irminger Sea applies to the past) during the last deglaciation. The same conclusion can be drawn from our low-resolution $\delta^{11}B$ record independently (Figure 6d).

[32] Our work does not fully constrain the role of the polar North Atlantic on CO_2 uptake during the last deglaciation, because *N. pachyderma* (s) only lives in certain seasons, if the modern observation in the North Atlantic applies to the past. To obtain the annual mean values of surface mixed layer properties, a perfect situation requires that (i) the species lives in the surface mixed layer during its entire life cycle, (ii) the species grows year round, (iii) the flux of shells of the species is evenly distributed during different seasons throughout the year and does not change through time, and (iv) the shells of the species calcified in each season are equally/proportionally preserved in the sediment. Unfortunately almost no species fulfills these criteria, and certainly not one found in the polar North Atlantic. Much work is therefore still needed to fully constrain the role of the polar North Atlantic in controlling atmospheric CO_2 in the past. However, we note that sediment trap studies from the northwestern North Pacific [*Kuroyanagi et al.*, 2011] found that *N. pachyderma* (s) appears to calcify year-around with roughly equal shell fluxes from contrasting seasons (spring versus autumn and summer versus winter) and non-flux-normalized $\delta^{18}O$ of shells matches the modern annual mean water value. This has led these authors to suggest that $\delta^{18}O$ of this species could represent the annual mean environments around the pycnocline under certain circumstances. We therefore encourage future studies to investigate the possible use of *N. pachyderma* (s) B/Ca and $\delta^{11}B$ to obtain estimates of past annual mean surface pCO_2 in the (sub) polar North Pacific.

10. Conclusion

[33] We have investigated B/Ca and $\delta^{11}B$ in *N. pachyderma* (s) as proxies to constrain changes in CO_2 uptake in the polar North Atlantic Ocean during the last deglaciation. We use *N. pachyderma* (s) as it is the only species from which we could obtain continuous deglacial B/Ca and $\delta^{11}B$ records. Our core-top results suggest roughly constant K_D and $\delta^{11}B_{cc\text{-}B4}$ associated with the incorporation of boron into *N. pachyderma* (s), with some scatter possibly attributable to the scarcity of suitable hydrographic data in the study region. Using $K_D = 1.48 \times 10^{-3}$ and $\delta^{11}B_{cc\text{-}B4} = -3.38‰$, seawater pH, CO_3^{2-}, and pCO_2 values derived from B/Ca and $\delta^{11}B$ in down-core records show similar trends and agree within reconstruction uncertainties. Both methods show subsurface pCO_2 has been lower than contemporary atmospheric CO_2 during 19–10 ka. The variability in down-core pCO_2 is significantly correlated with nutrient based on Cd/Ca. As surface pCO_2 are inevitably lower than subsurface values, our reconstructions suggest that the polar North Atlantic has remained a sink of CO_2 over the growth seasons of *N. pachyderma* (s) during the last deglaciation. Reconstructing past surface water pCO_2 is challenging and we suggest future studies such as culturing and sediment trap work to improve our understanding of boron incorporation into *N. pachyderma* (s).

[34] **Acknowledgments.** We thank T. Takahashi, R. Ryderson, H. Elderfield, and F. He for very helpful discussions, O. Hyams-Kaphzan, Z. Jin, M. Greaves, and Chris Coath for excellent lab assistance, and T. Dokken for providing three core-tops from the Norwegian Sea. We also thank constructive comments from two anonymous reviewers. This research is funded by Lamont-Doherty Postdoctoral Fellowship, Lawrence Livermore Fellowship and the Australian National University (J.Y.), by NERC RAPID grant NER/T/S/2002/00436 (N. M. and D. T.), and by a NERC PhD studentship (J.R.). The cores examined in this study were obtained during cruise CD-159 of RRS *Charles Darwin* funded by the RAPID Climate Change programme of NERC (UK).

References

Allen, K. A., and B. Hönisch (2012), The planktic foraminiferal B/Ca proxy for seawater carbonate chemistry: A critical evaluation, *Earth. Planet. Sci. Lett.*, *345–348*, 203–211.

Allen, K. A., et al. (2011), Controls on boron incorporation in cultured tests of the planktic foraminifer Orbulina universa, *Earth. Planet. Sci. Lett.*, *309*(3–4), 291–301.

Anderson, R. F., et al. (2009), Wind-driven upwelling in the Southern Ocean and the deglacial rise in atmospheric CO_2. *Science*, *323*, 1443–1448.

Azetsu-Scott, K., and F. C. Tan (1997), Oxygen isotope studies from Iceland to an East Greenland Fjord: Behaviour of glacial meltwater plume, *Mar. Chem.*, *56*, 239–251.

Barker, S., and H. Elderfield (2002), Foraminiferal calcification response to glacial-interglacial changes in atmospheric CO_2, *Science*, *297*(5582), 833–836.

Barker, S., M. Greaves, H. Elderfield (2003), A study of cleaning procedures used for foraminiferal Mg/Ca paleothermometry, *Geochem. Geophys. Geosyst.*, *4*(9), 8407.

Bauch, D., J. Carstens, and G. Wefer (1997), Oxygen isotope composition of living *Neogloboquadrina pachyderma* (sin.) in the Arctic Ocean, *Earth. Planet. Sci. Lett.*, *146*, 47–58.

Beer, C. J., R. Schiebel, and P. A. Wilson (2010), Testing planktic foraminiferal shell weight as a surface water [CO_3^{2-}] proxy using plankton net samples, *Geology*, *38*(2), 103–106.

Bian, N. X., and P. A. Martin (2010), Investigating the fidelity of Mg/Ca and other elemental data from reductively cleaned planktonic foraminifera, *Paleoceanography*, *25*, doi:10.1029/2009pa001796.

Boyle, E.A. (1983), Manganese carbonate overgrowths on foraminifera tests, *Geochim. Cosmochim. Acta*, *47*(10), 1815–1819.

Boyle, E. A., and L. D. Keigwin (1985/86), Comparison of Atlantic and Pacific paleochemical records for the last 215,000 years: Changes in deep ocean circulation and chemical inventories, *Earth Planet. Sci. Lett.*, *76*(1–2), 135–150.

Broecker, W. (1982), Glacial to interglacial changes in ocean chemistry, *Progr. Oceanogr.*, *2*, 151–197.

Broecker, W., and T. H. Peng (1992), Interhemispheric transport of carbon dioxide by ocean circulation, *Nature*, *356*, 587–589.

Broecker, W., T. H. Peng, S. Trumbore, G. Bonani, and W. Wolfli (1990), The distribution of radiocarbon in the glacial ocean, *Global Biogeochem. Cycles*, *4*(1), 103–117.

Dickson, A. G. (1990), Thermodynamics of the dissociation of boric-acid in synthetic seawater from 273.15K to 318.15K, *Deep-Sea Res. Part A-Oceanogr. Res. Pap.*, *37*(5), 755–766.

Dickson, A. G., and F. J. Millero (1987), A comparison of the equilibrium constants for the dissociation of carbonic acid in seawater media, *Deep-Sea Res.*, *34*, 1733–1743.

DOE (1994), *Handbook of Methods for the Analysis of the Various Parameters of the Carbon Dioxide System in Seawater*; version 2, Washington, D. C., ORNL/CDIAC-74.

Duplessy, J. C., et al. (1988), Deepwater source variations during the last climatic cycle and their impact on the global deepwater circulation, *Paleoceanography*, *3*(3), 343–360.

Elderfield, H., and R. E. M. Rickaby (2000), Oceanic Cd/P ratio and nutrient utilization in the glacial Southern Ocean, *Nature*, *405*(6784), 305–310.

Etheridge, D. M., et al. (1996), Natural and anthropogenic changes in atmospheric CO2 over the last 1000 years from air in Antarctic ice and firn, *J. Geophys. Res.-Atmos.*, *101*(D2), 4115–4128.

Feely, R. A., et al. (2004), Impact of anthropogenic CO_2 on the $CaCO_3$ system in the oceans, *Science*, *305*, 362–366.

Foster, G. L. (2008), Seawater pH, pCO_2 and [CO_3^{2-}] variations in the Caribbean Sea over the last 130 kyr; a boron isotope and B/Ca study of planktic foraminifera, *Earth Planet. Sci. Lett.*, *271*(1–4), 254–266. doi:10.1016/j.epsl.2008.04.015.

Foster, G. L., P. A. E. Pogge von Strandmann, and J. W. B. Rae (2010), Boron and magnesium isotopic composition of seawater. *Geochem. Geophys. Geosyst.*, *11*, doi:10.1029/2010gc003201.

Hain, M. P., D. M. Sigman, and G. H. Haug (2013), The Biological Pump in the Past, *Treatise on Geochemsitry* 2nd edition, pp. doi:10.1016/B978-0-08-095975-7.00618-5.

Hemming, N. G., and G. N. Hanson (1992), Boron isotopic composition and concentration in modern marine carbonates, *Geochim. Cosmochim. Acta*, *56*(1), 537–543.

Hendry, K. R., R. E. M. Rickaby, M. P. Meredith, and H. Elderfield (2009), Controls on stable isotope and trace metal uptake in *Neogloboquadrina pachyderma* (sinistral) from an Antarctic sea-ice environment, *Earth Planet. Sci. Lett.*, *278*(1–2), 67–77, doi:10.1016/j.epsl.2008.11.026.

Hillaire-Marcel, C., and A. de Vernal (2008), Stable isotope clue to episodic sea ice formation in the glacial North Atlantic, *Earth Planet. Sci. Lett.*, *268*(1–2),143–150.

Hönisch, B., T. Bickert, and N. G. Hemming (2008), Modern and Pleistocene boron isotope composition of the benthic foraminifer *Cibicidoides wuellerstorfi*, *Earth Planet. Sci. Lett.*, *272*, 309–318. doi:10.1016/j.epsl.2008.04.047.

Hönisch, B., et al. (2003), The influence of symbiont photosynthesis on the boron isotopic composition of foraminifera shells. *Mar. Micropaleontol.*, *49*(1–2), 87–96.

Hönisch, B., and N. G. Hemming (2005), Surface ocean pH response to variations in pCO_2 through two full glacial cycles, *Earth Planet. Sci. Lett.*, *236*(1–2), 305–314.

Jasper, J. P., J. M. Hayes, and E. L. Sikes (1995), Transfer of CO_2 from equatorial latitudes to high latitudes during the late Quaternary. In: B. Jahne and E. Monahan (Editors), Air-Water Gas Transfer. AEON Verlag, pp. 879–888.

Jonkers, L., G. J. A. Brummer, F. J. C. Peeters, H. M. van Aken, and M. F. De Jong (2010), Seasonal stratification, shell flux, and oxygen isotope dynamics of left-coiling *N. pachyderma* and *T. quinqueloba* in the western subpolar North Atlantic, *Paleoceanography*, *25*, PA2204, doi:10.1029/2009PA001849.

Keeling, C. D., and M. Heimann (1986), Meridional eddy diffusion model of the transport of atmospheric carbon dioxide 2. mean annual carbon cycle, *J. Geophys. Res.*, *91*(D7), 7782–7796.

Keeling, C. D., T. P. Whorf, and Group, t.C.D.R. (2004), Atmospheric CO_2 concentrations (ppmv) derived from in situ air samples collected at Mauna Loa Observatory, Hawaii, La Jolla.

Key, R. M., et al. (2004), A global ocean carbon climatology: Results from Global Data Analysis Project (GLODAP), *Global Biogeochem. Cycles*, *18*(4).

Kim, S., and J. R. O'Neil (1997), Equilibrium and nonequilibrium oxygen isotope effects in synthetic carbonates, *Geochim. Cosmochim. Acta*, *61*(16), 3461–3475.

Klochko, K., G. D. Cody, J. A. Tossell, P. Dera, and A. J. Kaufman (2009), Re-evaluating boron speciation in biogenic calcite and aragonite using ^{11}B MAS NMR, *Geochim. Cosmochim. Acta*, *73*, 1890–1900.

Klochko, K., A. J. Kaufman, W. Yao, R. H. Byrne, and J. A. Tossell (2006), Experimental measurement of boron isotope fractionation in seawater. *Earth Planet. Sci. Lett.*, *248*, 276–285.

Kohfeld, K. E., R. F. Anderson, and J. Lynch-Stieglitz (2000), Carbon isotopic disequilibrium in polar planktonic foraminifera and its impact on modern and Last Glacial Maximum reconstructions, *Paleoceanography*, *15*(1), 53–64.

Kristjánsdóttir, G. B., C. Bryant, H. Elderfield, and I. N. McCave (2011), AMS C-14 ages of coretops collected on RRS Charles Darwin cruise CD159, July 2004, N. Atlantic, for the NERC RAPID programme. PANGAEA Dataset #773254: doi:10.1594/PANGAEA.773254.

Kuroyanagi, A., H. Kawahata, and H. Nishi (2011), Seasonal variation in the oxygen isotopic composition of different-sized planktonic foraminifer Neogloboquadrina pachyderma (sinistral) in the northwestern North Pacific and implications for reconstruction of the paleoenvironment, *Paleoceanography*, *26*, doi:10.1029/2011pa002153.

Lee, K., et al. (2010), The universal ratio of boron to chlorinity for the North Pacific and North Atlantic oceans, *Geochim. Cosmochim. Acta*, *74*, 1801–1811.

Lee, K., et al. (2006), Global relationships of total alkalinity with salinity and temperature in surface waters of the world's oceans, *Geophys. Res. Lett.*, *33*, L19605, doi:10.1029/2006GL027207.

LeGrande, A. N., and G. A. Schmidt (2006), Global gridded data set of the oxygen isotopic composition in seawater, *Geophys. Res. Lett.*, *33*(12), doi:10.1029/2006gl026011.

Lemieux-Dudon, B., et al. (2010), Consistent dating for Antarctic and Greenland ice cores, *Quat. Sci. Rev.*, *29*, 8–20.

Lynch-Stieglitz, J., T. F. Stocker, W. Broecker, and R. G. Fairbanks (1995), The influence of air-sea exchange on the isotopic composition of oceanic carbon: Observations and modeling, *Global Biogeochem. Cycles*, *9*(4), 653–665.

Maslin, M. A., E. Thomas, N. J. Shackleton, M. A. Hall, and D. Seidov (1997), Glacial northeast Atlantic surface water p(CO2): Productivity and deep-water formation, *Mar. Geol.*, *144*(1–3), 177–190.

Mehrbach, C., C. H. Culberso, J. E. Hawley, and R. M. Pytkowic (1973), Measurement of apparent dissociation-constants of carbonic-acid in seawater at atmospheric-pressure, *Limnol. Oceanogr.*, *18*(6), 897–907.

Monnin, E., et al. (2001), Atmospheric CO_2 Concentrations over the Last Glacial Termination, *Science*, *291*, 112–114.

Nyland, B. F., E. Jansen, H. Elderfield, and C. Andersson (2006), Neogloboquadrina pachyderma (dex. and sin.) Mg/Ca and delta(18)O records from the Norwegian Sea, *Geochem. Geophys. Geosyst.*, *7*, doi:10.1029/2005gc001055.

Palmer, M. R., et al. (2010), Multi-proxy reconstruction of surface water pCO2 in the northern Arabian Sea since 29 ka, *Earth Planet. Sci. Lett.*, *295*, 49–57.

Palmer, M. R., and P. N. Pearson (2003), A 23,000-year record of surface water pH and PCO_2 in the western equatorial Pacific Ocean, *Science*, *300*(5618), 480–482.

Pelletier, G., E. Lewis, and D. Wallace (2005), A calculator for the CO_2 system in seawater for Microsoft Excel/VBA. Washington State Department of Ecology, Olympia, WA, Brookhaven National Laboratory, Upton, NY.

Pflaumann, U., et al. (2003), Glacial North Atlantic: Sea-surface conditions reconstructed by GLAMAP 2000, *Paleoceanography*, *18*(3), doi:10.1029/2002PA000774.

Rae, J. W. B., G. L. Foster, D. N. Schmidt, and T. Elliott (2011), Boron isotopes and B/Ca in benthic foraminifera: Proxies for the deep ocean carbonate system, *Earth Planet. Sci. Lett.*, *302*(3–4), 403–413.

Rasmussen, S. O., et al. (2006), A new Greenland ice core chronology for the last glacial termination, *J. Geophys. Res.-Atmos.*, *111*(D6), D06102.

Rickaby, R. E. M., and H. Elderfield (1999), Planktonic foraminiferal Cd/Ca: Paleonutrients or paleotemperature? *Paleoceanography*, *14*(3), 293–303.

Rickaby, R. E. M., and H. Elderfield (2005), Evidence from the high-latitude North Atlantic for variations in Antarctic Intermediate water flow during the last deglaciation, *Geochem. Geophys. Geosyst.*, *6*, Q05001, doi:10.1029/2004GC000858.

Sanyal, A., N. G. Hemming, W. S. Broecker, and G. N. Hanson (1997), Changes in pH in the eastern equatorial Pacific across stage 5–6 boundary based on boron isotopes in foraminifera, *Global Biogeochem. Cycles*, *11*(1), 125–133.

Sanyal, A., et al. (1996), Oceanic pH control on the boron isotopic composition of foraminifera: Evidence from culture experiments, *Paleoceanography*, *11*(5), 513–517.

Sarmiento, J. L., N. Gruber, M. A. Brzezinski, and J. P. Dunne (2003), High-latitude controls of thermocline nutrients and low latitude biological productivity, *Nature*, *427*, 56–60.

Schlitzer, R. (2006), Ocean Data View. http://odv.awi-bremerhaven.de.

Schmidt, M. W., H. J. Spero, and D. W. Lea (2004), Links between salinity variation in the Caribbean and North Atlantic thermohaline circulation. *Nature*, *428*, 160–163.

Sigman, D. M., and E. A. Boyle (2000), Glacial/interglacial variations in atmospheric carbon dioxide, *Nature*, *407*(6806), 859–869.

Simstich, J., M. Sarnthein, and H. Erlenkeuser (2003), Paired $\delta^{18}O$ signals of *Neogloboquadrina pachyderma* (s) and *Turborotalita quinqueloba* show thermal stratification structure in Nordic Seas, *Mar. Micropalentology*, *48*, 107–125.

Takahashi, T., J. Olafsson, J. G. Goddard, D. W. Chipman, and S. C. Sutherland (1993), Seasonal variation of CO_2 and nutrients in the high-latitude surface oceans: A comparative study. *Global Biogeochem. Cycles*, *7*(4), 843–878.

Takahashi, T., et al. (2002), Global sea-air CO_2 flux based on climatological surface ocean pCO_2, and seasonal biological and temperature effects, *Deep-Sea Res. II*, *49*, 1601–1622.

Takahashi, T., et al. (2009), Climatological mean and decadal change in surface ocean pCO(2), and net sea-air CO2 flux over the global oceans, *Deep-Sea Res. Part Ii-Topical Stud. Oceanography*, *56*(8–10), 554–577.

Thornalley, D. J. R., S. Barker, W. Broecker, H. Elderfield, and I. N. McCave (2011a), The deglacial evolution of North Atlantic Deep Convection, *Science*, *331*, 202–205.

Thornalley, D. J. R., H. Elderfield, and I. N. McCave (2010), Intermediate and deep water paleoceanography of the northern North Atlantic over the past 21,000 years, *Paleoceanography*, *25*, PA1211, doi:10.1029/2009PA001833.

Thornalley, D. J. R., H. Elderfield, and I. N. McCave (2011b), Reconstructing deglacial North Atlantic surface hydrography and its link to the Atlantic overturning circulation, *Global and Planet. Change*, doi:10.1016/j.gloplacha.2010.06.003.

Yu, J., et al. (2010), Loss of carbon from the deep sea since the Last Glacial Maximum, *Science*, *330*, 1084–1087, doi:10.1126/science.1193221.

Yu, J. M., J. Day, M. Greaves, and H. Elderfield (2005), Determination of multiple element/calcium ratios in foraminiferal calcite by quadrupole ICP-MS, *Geochem. Geophys. Geosyst.*, *6*, Q08P01, doi:10.1029/2005GC000964.

Yu, J. M., and H. Elderfield (2007), Benthic foraminiferal B/Ca ratios reflect deep water carbonate saturation state, *Earth. Planet. Sci. Lett.*, *258*(1–2), 73–86, doi:10.1016/j.epsl.2007.03.025.

Yu, J. M., H. Elderfield, M. Greaves, and J. Day (2007a), Preferential dissolution of benthic foraminiferal calcite during laboratory reductive cleaning, *Geochem. Geophys. Geosyst.*, *8*, Q06016, doi:10.1029/2006GC001571.

Yu, J. M., H. Elderfield, and B. Honisch (2007b), B/Ca in planktonic foraminifera as a proxy for surface seawater pH, *Paleoceanography*, *22*(2), PA2202, doi:10.1029/2006PA001347.

Zeebe, R. E., D. A. Wolf-Gladrow, J. Bijma, and B. Hönisch (2003), Vital effects in foraminifera do not compromise the use of $\delta^{11}B$ as a paleo-pH indicator: Evidence from modeling, *Paleoceanography*, *18*(2), doi:10.1029/2003PA000881.